Kent Academic Repository

Xu, Weicheng, Yan, Yong, Huang, Xiaobin and Hu, Yonghui (2022) *Quantitative Measurement of the Stability of a Pulverized Coal Fired Flame through Digital Image Processing and Statistical Analysis.* **Measurement . ISSN 0263-2241. (In press)**

Quantitative Measurement of the Stability of a Pulverized Coal Fired Flame through Digital Image Processing and Statistical Analysis

Abstract

The stability of pulverized coal flames is a well-known problem in the power industry. Unstable flames often lead to lower combustion efficiency, higher pollutant emissions, and other operational problems. Many methods are available for flame monitoring and characterization, but very few are suitable for flame stability monitoring. This paper presents a method for assessing flame stability continuously and quantitatively by introducing a term named numerical indicator of flame stability based on digital image processing. This numerical indicator combines the statistical characteristics of four flame parameters which are derived from the flame images. To evaluate the effectiveness of the proposed method, the numerical indicator of a pulverized coal flame during a routine unit "turning off" process was determined on a 600 MWth coal-fired supercritical unit. Experimental results suggest that the flame stability at different stages of the turning off process is correctly quantified with the numerical indicator.

Keywords: Pulverized coal; Flame stability; Flame monitoring; Digital imaging; Image processing; Statistical analysis.

1. Introduction

Flame stability in pulverized coal combustion is becoming increasingly an area of concern due to the trends of extending the use of low-quality coal and coal blends in existing power industries [1]. An unstable flame can cause many combustion problems, such as furnace vibration, low combustion efficiency, high NOx emissions, and even flameouts [2]. To improve overall performance of the furnace, ensure the safety of operators, and meet the stringent standards on energy saving and pollutant emissions, monitoring and characterization of flame stability have become highly desirable in the power generation industry [3].

Various techniques for flame stability assessment have been proposed, such as planar laser-induced fluorescence [4, 5], chemiluminescence imaging [6, 7], electrostatic sensing [8, 9], and digital imaging [10, 11]. Digital imaging has been identified as one of the most effective approaches for flame stability assessment in practical furnaces in terms of system functionality, portability, cost-effectiveness and rich information [3]. Wojcik et al. [12] measured the stability of flames on a pulverized coal-fired furnace at a power industry by analysing the flame radiation images filtered by the wavelet transform. Smart et al. [13] investigated the stability of an oxy-fuel flame on a 0.5 MWth coal fired combustion test rig by analysing the oscillation frequency of the radiation intensity of the root region of the flame. Samantaray et al. [14] analysed the stability of a natural gas flame and a coal-biomass co-firing flame in a 0.5 MWth pulverized fuel fired pilot swirl combustor through the uniformity of the two-dimensional distribution of flame brightness for studying the stability diagram of the flame. Matthes et al. [15] used the variation rate of the edges of a pulverized coal flame in a 2.5 MWth pilot swirl combustor to characterize the flame stability. Most of the existing flame stability measurement methods based on image processing use a single flame feature, such as contour [16, 17], root area [18, 19], colour [20, 21], and oscillation frequency [22, 23]. There are many limitations in these methods. It is impossible to extract flame contours from the image if the flame occupies the whole field of view of the camera [24]. Due to the limitation of the installation position of the camera on a coal fired unit in the power industry, the whole root of a flame may not be observed [25]. These methods focus on the stable state of a flame on their specific perspectives, which cannot reflect the real flame stability. There are some methods which evaluate flame stability through combining multiple parameters [26, 27]. But on the one hand, some parameters which contain flame stability information may be omitted during the combination [26]; on the other hand, under specific combustion conditions, the parameters used in the

combination may not reflect the flame stability, which should be excluded [27].

This research focuses on the continuous and quantitative measurement of pulverized coal flame stability through digital image processing. The characteristic parameters of the flame, including brightness, nonuniformity, mean temperature, and oscillation frequency, are derived from flame images. The statistical characteristics of these parameters are combined to provide a numerical indicator for evaluating the flame stability. The findings reported in this paper are linked to the earlier work on the development of a general methodology for flame stability measurement [28]. In the earlier work, the quantitative measurement of the stability of a premixed methane-air flame and a methane-biomass flame has demonstrated the effectiveness of the general methodology. The applicability of this general methodology under a wide range of combustion conditions remains to be investigated.

The novelty of this paper lies in the quantitative measurement of the stability of a pulverized coal flame under full-scale power station conditions. The combustion of pulverized coal is far more complex than that of methane and biomass due to its complex physical and chemical properties [29, 30], and hence the measurement of the stability of a pulverized coal flame is more challenging. Furthermore, unlike on a laboratory combustion test rig, the harsh environment in a full-scale power plant furnace, such as high temperature and fly ash [31], make the measurement of pulverized coal flame stability more difficult. In addition, algorithms for advanced flame stability measurement in the power generation industry are still limited. Therefore, the evaluation of the proposed methodology for flame stability assessment on a full-scale coal fired power plant has important practical significance. It is anticipated that this method, once validated, will assist the power plant operators to measure quantitatively the flame stability and
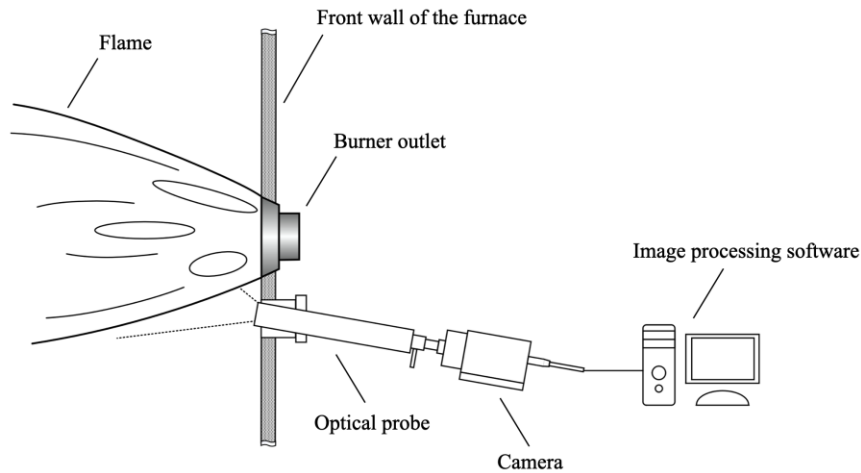
Fig. 1. Installation of the imaging system for flame stability measurement.
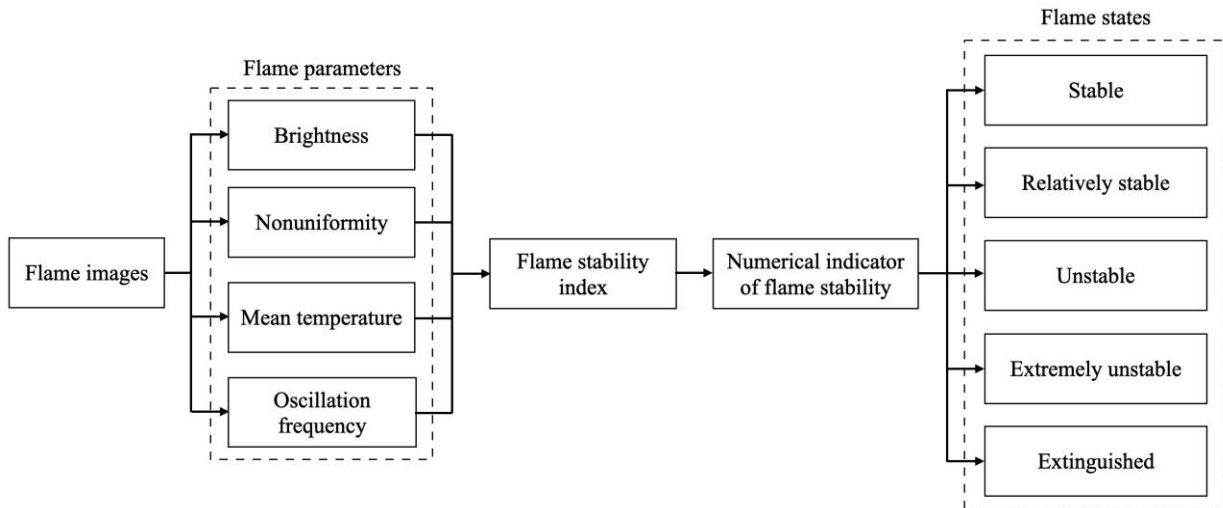
Fig. 2. Block diagram of the flame stability assessment method.

identify the flame state and ultimately to optimize power plant operation.

2. Methodology

2.1. Measurement principle

Fig. 1 shows a block diagram of the typical installation of the imaging system for flame stability measurement. The system consists of an optical probe, a CCD camera and a computer with bespoke image processing software. The optical probe, installed at an existing viewing port on the back of the burner, transmits the images of the root region of the flame to the camera. The image processing software processes the images and derives quantified flame stability continuously. Fig. 2 shows a block diagram of the flame stability measurement method. Four flame characteristic parameters, i.e., brightness, nonuniformity, mean temperature and oscillation frequency, are derived from the flame images using various digital image processing algorithms. The statistical characteristics of the four parameters are combined to obtain a flame stability index, which quantifies flame stability preliminarily. Then the index is converted to an integer as a numerical indicator of flame stability. This indicator is a single digit ranging from 0 to 10 and represents one of the five flame states, i.e., stable, relatively stable, unstable, extremely unstable, and extinguished. The numerical indicator of flame stability is convenient for power plant operators to quantify flame stability information.

Since the flame image is a two-dimensional projection of the burner flame which is three-dimensional in space, the installation position of the imaging probe affects significantly the image representation of the flame and the quality of the images. An ideal installation position under labotoray conditions is on the side-wall of the furnace where the camera can capture the side view of the whole flame. However, there are many constraints on a full-scale power station furnace where we can only install the imaging probe on a viewing port which is located at the back of the burner. This location is not ideal but the best we can do on a real power plant. However, with the imaging system we are able to visualize the root region of the flame, the most important part of the flame. Compared to the well-established flame-eyes or similar devices which "see" only a single line across a flame, the imaging approach provides significantly more information about the flame. Meanwhile, there are advantages to install the imaging probe at the back of the burner as this will ensure the camera visualises only the flame to be monitored and is not affected by neighboring flames in a multi-burner furnace. It is worth noting that, for the given existing viewing port (Fig. 1), the angle of the probe to the flame is almost fixed and a slight variation has no significant effect on the quality of the images collected and flame stability result.

In this study, the term 'flame stability' is defined as the degree of fluctuation of a flame due to all physical and chemical changes in the flame characteristics during combustion. The stability of a flame depends on a variety of flame characteristics, including geometrical, thermodynamic and optical properties which in turn depend on many other factors such as type of fuel, fuel quality, burner design and combustion environment (air supply, furnace structure etc.). This study aims to measure quantitatively the stability of the coal fired flame under full-scale power station conditions. The ultimate aim of retaining stable flames is to optimize the combustion process, i.e., high combustion efficiency, low pollutant emissions, and enhance plant safety, under a wide range of plant conditions.

2.2. Flame parameters

The measurement of the flame parameters depends upon many factors, such as fuel type, burner type, furnace structure, and installation position of the imaging probe. Practical constraints on a full-scale power plant (e.g. line-of-sight restrictions, availability of a viewing port, burner structure etc.) often make the imaging probe installed on a less ideal of position, and therefore certain flame parameters may not be available. Since there are always some parameters available such as brightness, nonuniformity, temperature distribution etc, regardless of the installation position, the method presented in this paper is useful for evaluating flame stability.

In the case of the present research, because the installation of the probe and hence the view of the flame depend on the availability of the observation port and furnace design, as shown in Fig. 1, some of the parameters are not measurable such as ignition point. The ignition point can be measured only when the fuel is ignited beyond the burner outlet. Furthermore, some of the parameters such as flame area and flame length are not concerned by

the operator, although their variation characteristics may include important information about flame stability. According to the characteristic of the flame images, the following four parameters are measured:

(1) *Brightness* is defined as the average luminosity of a flame, normalized to the maximum grey-level of an 8-bit digital image, i.e., 255. The brightness reflects the most basic luminous characteristics of the flame.

(2) *Nonuniformity* represents the luminosity deviation between the 'darker' and 'brighter' regions of a flame. The nonuniformity reflects the uniformity of heat release in the flame region.

(3) *Mean temperature* is the spatial average of the temperature distribution over the area of a flame image. The temperature distribution is determined using the radiation method [32]. The variation in the temperature distribution reflects the process of radiative heat transfer and is closely related to flame stability. The mean temperature characterizes the flame temperature distribution to a certain degree.

(4) *Oscillation frequency* is determined as the weighted average frequency of the power-density of the flame signal (in the whole frequency range). The low-frequency components of a flame signal stem largely from the geometrical fluctuations of the flame due to the aerodynamic or convective effect, whilst high-frequency components may be because of the energy transitions among intermediate radicals or variations in the energy emission rate of reacting species [33]. Flame oscillation frequency is a comprehensive characteristic parameter which is closely related to flame stability.

Detailed definitions of these parameters are given elsewhere [28]. Based on the definitions, the four parameters are derived from flame images. A flowchart for the determination of the flame parameters is shown in Fig. 3. The RGB (red, green, and blue) images of a flame, which are captured by the camera, are converted into greyscale images via the following equation [34],

$$I = 0.30R + 0.59G + 0.11B \qquad (1)$$

where R, G, and B are red, green, and blue components in RGB colour space, respectively, and I is a weighted sum of the three individual components in the RGB colour space and represents the radiation intensity distribution of the flame. Then the greyscale images are converted into binary

images based on the adapting thresholding technique [35]. The binary images are used to analyse the geometric characteristics of the flame. Finally, the four parameters are determined from the greyscale and binary images together.

It should be emphasized that the method presented in this paper extracts all possible flame characteristic parameters from the images and integrates them to determine flame stability. In other words, which parameters are determined and combined is not fixed because the measurement of the parameters depends on
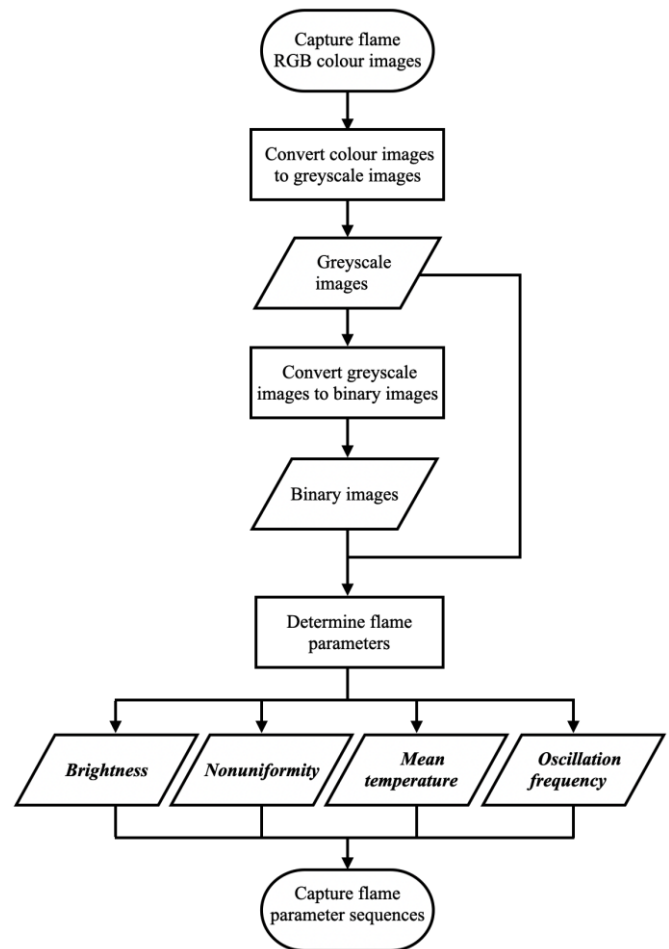
Fig. 3. Flowchart for the determination of flame parameters from flame images.

many factors. If a flame parameter is not available, then this parameter will not be quantified and used in the flame stability measurement.

2.3. Flame stability index

Flame stability index, which has been previously reported to evaluate the stabilities of methane and biomass flames [28], is used to measure the pulverized coal flame stability in this study. Fig.4 shows a flowchart of the software for the determination of flame stability index. Methane, biomass and coal are different fuels and their burners and furnaces are also different. The imaging system measures flame stability for a given combustion setting, regardless of fuel, burner and furnace, i.e., the same general procedure is applied to measure flame stability. However, since combustion setting is different from one system to another, there bound to be some differences between them when we apply the same procedure. In the case of the methane flame [28], its stability evaluation combines the flame area, area of root region, mean temperature, and oscillation frequency, while the pulverized coal flame has brightness, nonuniformity, mean temperature, and oscillation frequency. The reason for such differences is that the methane flame was visualized with the camera on an optimal position under laboratory conditions and its colour changes with air flow rate, which is very different from the pulverized coal flame. In the case of the biomass flame [28], its stability combines the parameters including brightness, mean temperature and oscillation frequency, which are similar to those for the pulverized coal flame.

The flowchart in Fig. 4 is generic and is applicable to different flames. The values of a flame parameter are split into two groups: one group lies in the range between ± two standard deviations from the mean with 95% confidence limits, which is defined as usual values, while the other group is defined as unusual values, which fall outside ± two standard deviations. The normal and abnormal variability is obtained from the usual and unusual values, respectively. The normal variability of parameter x (δ_{x-nor}) is defined as

$$\delta_{x-nor} = \frac{\sigma_{x-nor}}{\mu_{x-nor}} \tag{2}$$

where σ_{x-nor} and μ_{x-nor} are the standard deviation and mean of the usual values of the parameter x, respectively. δ_{x-nor}
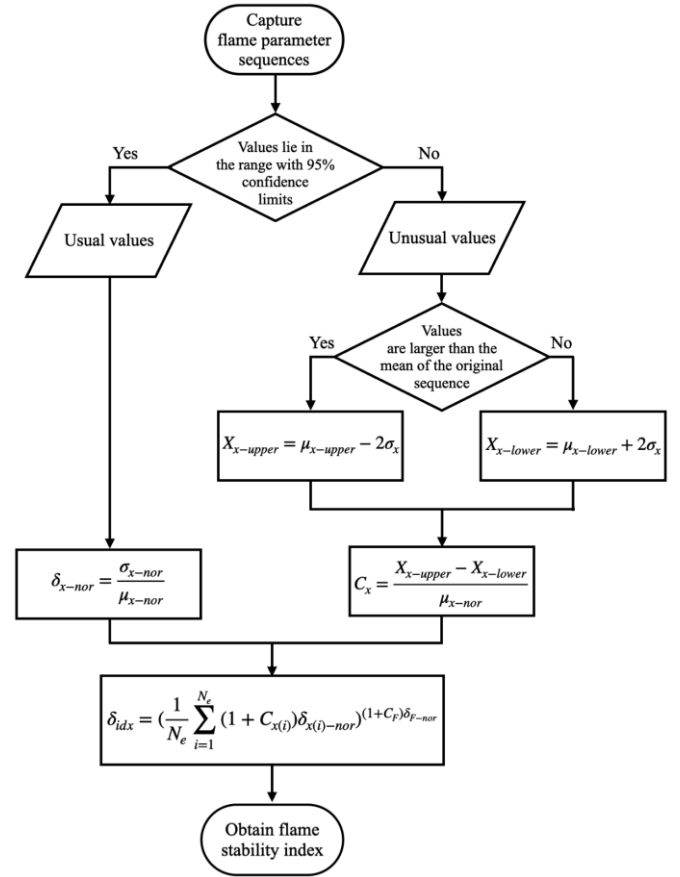
Fig. 4. Flowchart for the determination of flame stability index.

reflects the most common and basic characteristics of the flame as a relative quantity.

The abnormal variability of parameter x ($\delta_{x-abnor}$) is quantified in terms of an instability coefficient (C_x) and the normal variability, i.e.,

$$\delta_{x-abnor} = C_x \delta_{x-nor} \tag{3}$$

where C_x represents the variability of the unusual values of the parameter x and is determined as,

$$C_x = \frac{X_{x-upper} - X_{x-lower}}{\mu_{x-nor}} \tag{4}$$

where $X_{x-upper}$ and $X_{x-lower}$ are calculated as follows:

$$X_{x-upper} = \mu_{x-upper} - 2\sigma_x \tag{5}$$

$$X_{x-lower} = \mu_{x-lower} + 2\sigma_x \tag{6}$$

where $\mu_{x-upper}$ and $\mu_{x-lower}$ are averages of the unusual values which lie in the ranges within the upper and lower 95% confidence limits, respectively. σ_x is the standard deviation of x. C_x is determined as the flame is stable. The abnormal variability reflects the sensitivity of a parameter to the change in flame stability.

The flame stability index (δ_{idx}) is determined by

$$\delta_{idx} = \left(\frac{1}{N_e} \sum_{i=1}^{N_e} (1 + C_{x(i)}) \delta_{x(i)-nor} \right)^{(1+C_F)\delta_{F-nor}} \quad (7)$$

where N_e is the number of the parameters used in determining the flame stability index, $x(i)$ is the ith parameter, $C_{x(i)}$ and $\delta_{x(i)-nor}$ are the instability coefficient and normal variability of $x(i)$, respectively. C_F and δ_{F-nor} are the instability coefficient and normal variability of the oscillation frequency, respectively. An increasing δ means that one or more parameters vary substantially, i.e., the flame is unstable. The closer the index to zero, the more stable the flame. Additionally, in view of the fact that the stability index cannot be zero due to the natural fluctuation of a flame, we use zero value index to represent the non-flame state, i.e. when the flame is extinguished.

2.4. Numerical indicator of flame stability

The flame stability index is always large than zero in practice, because the levels of characteristic parameters vary constantly even if the flame has achieved its most stable state. Due to no theoretical upper limit of the flame stability index, it is difficult for the industry operators to judge the real stable state of a flame using the stability index. Furthermore, small changes in the stability index means little to the operators because slight fluctuation in the flame stability in industrial furnaces is normal. In view of these facts, we need something simpler than stability index.

In an industrial furnace, as the flame stability meets the industrial demand and fluctuates slightly, the mean of the corresponding stability index is considered as the representation of the best flame stability under current combustion conditions. When the combustion conditions change, the stability index may decrease with a large or small standard deviation. A large standard deviation indicates deteriorating flame stability while a small standard deviation suggests that the flame has better stability and the representation of the best flame stability should be re-determined. Deteriorating flame stability can also be reflected in increasing stability index. Based on such a characteristic of the flame stability index, a numerical indicator of flame stability (δ_{idr}) is defined as follows

$$\delta_{idr} = \begin{cases} 5-\alpha_{idr} & if \ \delta_{idx} > 3\mu_{idx-stable} \\ 6-\alpha_{idr} & if \ 1.5\mu_{idx-stable} < \delta_{idx} \le 3\mu_{idx-stable} \\ 7-\alpha_{idr} & if \ \mu_{idx-stable} + 4\sigma_{idx-stable} < \delta_{idx} \le 1.5\mu_{idx-stable} \\ 8-\alpha_{idr} & if \ \mu_{idx-stable} + 3\sigma_{idx-stable} < \delta_{idx} \le \mu_{idx-stable} + 4\sigma_{idx-stable} \\ 9-\alpha_{idr} & if \ \mu_{idx-stable} + 2\sigma_{idx-stable} < \delta_{idx} \le \mu_{idx-stable} + 3\sigma_{idx-stable} \\ 10-\alpha_{idr} & if \ \mu_{idx-stable} - 2\sigma_{idx-stable} \le \delta_{idx} \le \mu_{idx-stable} + 2\sigma_{idx-stable} \\ 9-\alpha_{idr} & if \ \mu_{idx-stable} - 3\sigma_{idx-stable} \le \delta_{idx} < \mu_{idx-stable} - 2\sigma_{idx-stable} \\ 8-\alpha_{idr} & if \ \mu_{idx-stable} - 4\sigma_{idx-stable} \le \delta_{idx} < \mu_{idx-stable} - 3\sigma_{idx-stable} \\ 5-\alpha_{idr} & if \ 0.5\mu_{idx-stable} \le \delta_{idx} < \mu_{idx-stable} - 4\sigma_{idx-stable} \\ 3-\alpha_{idr} & if \ \delta_{idx} < 0.5\mu_{idx-stable} \end{cases} \quad (8)$$

where $\sigma_{idx-stable}$ and $\mu_{idx-stable}$ are the standard deviation and mean of the flame stability index as the flame is stable; α_{idr} is defined as follows

$$\alpha_{idr} = \begin{cases} 0 & if \ \sigma_{idx} < \sigma_{idx-stable} \\ 1 & if \ \sigma_{idx-stable} \le \sigma_{idx} < 2\sigma_{idx-stable} \\ 2 & if \ 2\sigma_{idx-stable} \le \sigma_{idx} < 10\sigma_{idx-stable} \\ 4 & if \ 10\sigma_{idx-stable} \le \sigma_{idx} < 50\sigma_{idx-stable} \\ 6 & if \ \sigma_{idx} \ge 50\sigma_{idx-stable} \end{cases} \quad (9)$$

where σ_{idx} is the standard deviation of the flame stability index. Equations (8) and (9) are derived from our long-term experimental observations and experience in monitoring a range of flames over the years. In general, a more stable flame fluctuates less. The numerical indicator of flame stability is in effect an integer converted and rounded from the flame stability index and ranges from 0 to 10. A smaller numerical indicator indicates that the flame is more unstable. The detailed relationship between the numerical indicator and stable states of a flame is as follows

(1) the flame is stable, when $\delta_{idr} \in [8, 10]$;

(2) the flame is relatively stable, when $\delta_{idr} \in [6, 8)$;

(3) the flame is unstable, when $\delta_{idr} \in [3, 6)$;

(4) the flame is extremely unstable, when $\delta_{idr} \in (0, 3)$;

(5) the flame is extinguished, when δ_{idr} is 0.

3. Demonstration trials and results

3.1. Combustion conditions and fuel property

Experimental work was undertaken on a 600 MWth coal-fired supercritical unit by firing pulverized coal to evaluate the effectiveness of the proposed methodology for numerical assessment of flame stability. An optical probe, shielded with a water-cooled jacket, was installed at an existing viewing port on the burner peripheral to visualize the flame using a 1/3-in RGB (red, green, blue) industrial CCD camera with 0.5-million pixels (960 width × 576 height). The objective lens of the probe has a 90-viewing

Table 1

Proximate and ultimate analysis of the pulverized coal (as received).

Proximate Analysis (%)	
Moisture content	6.70
Volatile matter content	39.67
Ash content	26.67
Others	26.96
Ultimate analysis (%)	
C	55.06
O	6.68
H	3.63
S	0.32
N	0.94
Others	33.37

angle with its surface being kept dust-free by a purged airflow. The root region of the flame is captured by the camera at a rate of 60 frames per second. It is known from our previous research that a pulverized coal flame spreads over a range of frequencies, but they are concentrated within the lower frequency band (0 to 20 Hz). The other factor that was considered when choosing the camera in terms of resolution and frame rate is its cost and the volume of the images to be processed by the computer. The flame images are acquired with 24-bit digitization (8 bits/channel).

Table 1 summarizes the proximate and ultimate analysis of the pulverized coal. In this research, the stability of the flame during a routine boiler "turning off" process is measured, the duration of which is 25 min. The reason for selecting this particular process is that the plant operators know well about the flame fluctuations (stability) during this procedure. More importantly, the field trials did not affect the routine operation of the power plant. The coal feed rate and air flow rate in this process are plotted in Fig. 5. The coal feed rate decreases rapidly from 11 min 30 sec to 16 min. The air flow rate begins to reduce at 15 min which is designed to be later than the coal feed rate for safety reasons. The "turning off" process is divided into four stages with time as depicted in Fig. 6. Fig. 7 shows typical flame images during the four stages of the process. Note that the flame images captured in 0 min-6 min and 21 min-25 min are not given here because of the fixed coal feed rate during the first and last stages. It can be seen in Fig. 7 that the flame is stable in the first stage where coal feed rate is constant. In the second stage, the
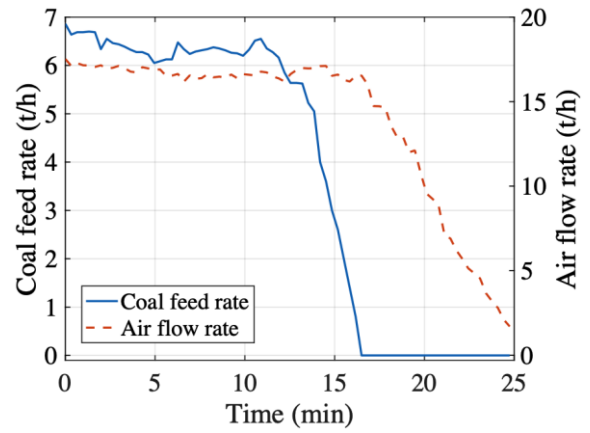
Fig. 5. Variations in the coal feed rate and air flow rate with time.

flame stability deteriorates rapidly. With further reduction in coal feed rate, i.e. the third stage, the flame fluctuates progressively towards extinction. Finally, in the last stage, the flame is extinguished as no coal feed.

3.2. Results and discussion

Fig. 8 shows the key stages in the processing of a typical flame image during the stage of constant coal feed rate. First, the original image, which is an average of 60 successive images taken in one second, is converted into the greyscale image based on equation (1). The original greyscale histogram is obtained from the greyscale image. Second, map the greyscale levels in the original greyscale histogram to the new levels (Fig. 8). The bottom 1% and top 1% of the greyscale levels of all pixels are set to saturation, i.e. 0 and 255, respectively, to increase the contrast of the greyscale image. Third, the binary image is determined from the processed greyscale image through the locally adaptive threshold method [35]. The threshold for each pixel is determined from the local mean greyscale level around the neighbourhood of the pixel, the size of which is approximately $1/8^{th}$ of the size of the image (69120 pixels in this study). Fourth, the flame edge is detected using the gradient-magnitude edge detection method [36]. A pair of 3×3 convolution masks are used to identify the edge by estimating the gradients in the X-direction and Y-direction, respectively. Last, the flame parameters, i.e. brightness, nonuniformity, mean temperature and oscillation frequency, are determined from the greyscale levels in the original greyscale image and information from the flame edge. Fig. 9 depicts typical flame images during the last three stages of the shutting off process (typical flame images during the first stage are
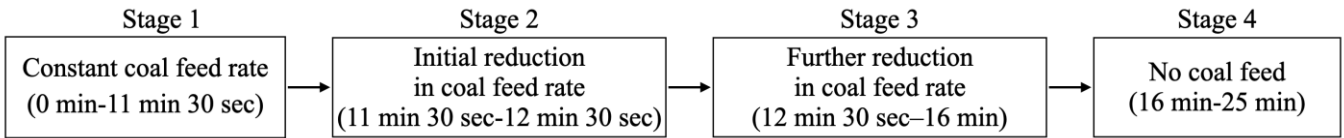
Fig. 6. Routine boiler "turning off" process.
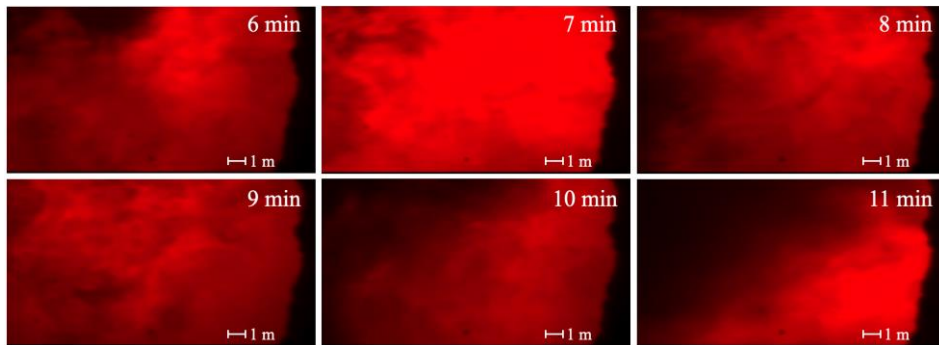
(a) Constant coal feed rate
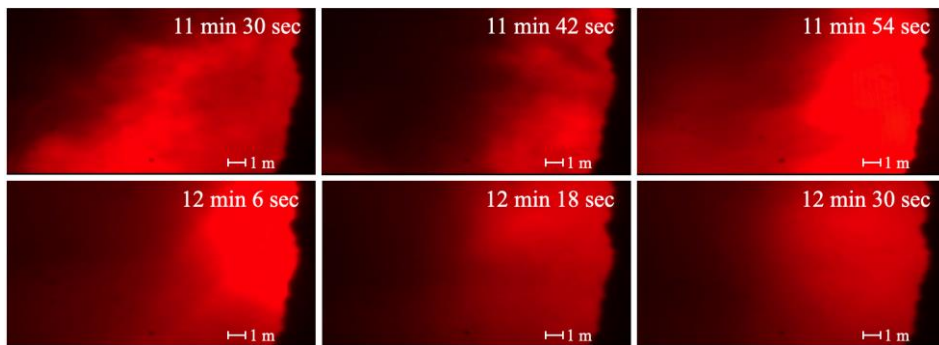
(b) Initial reduction in coal feed rate
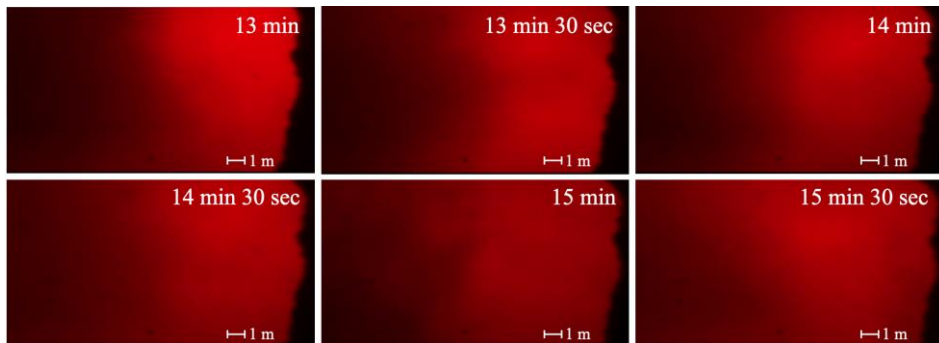
(c) Further reduction in coal feed rate
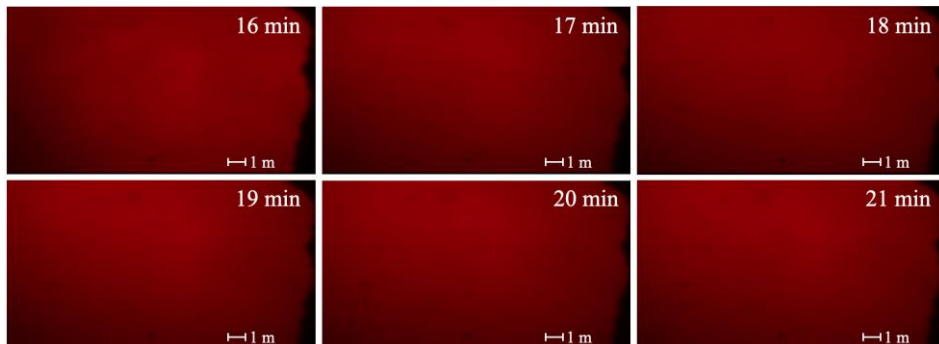
(d) No coal feed

Fig. 7. Typical flame images for different coal feed rates.

shown in Fig. 8). As can be seen in Figs. 8 and 9, during the first and second stages the flame edges are clear, whilst these edges gradually blur with rapidly decreasing coal feed rate during the third stage. In the last stage, no edges can be observed due to no coal feed. To a certain extent the flame edge information reflects the flame states.
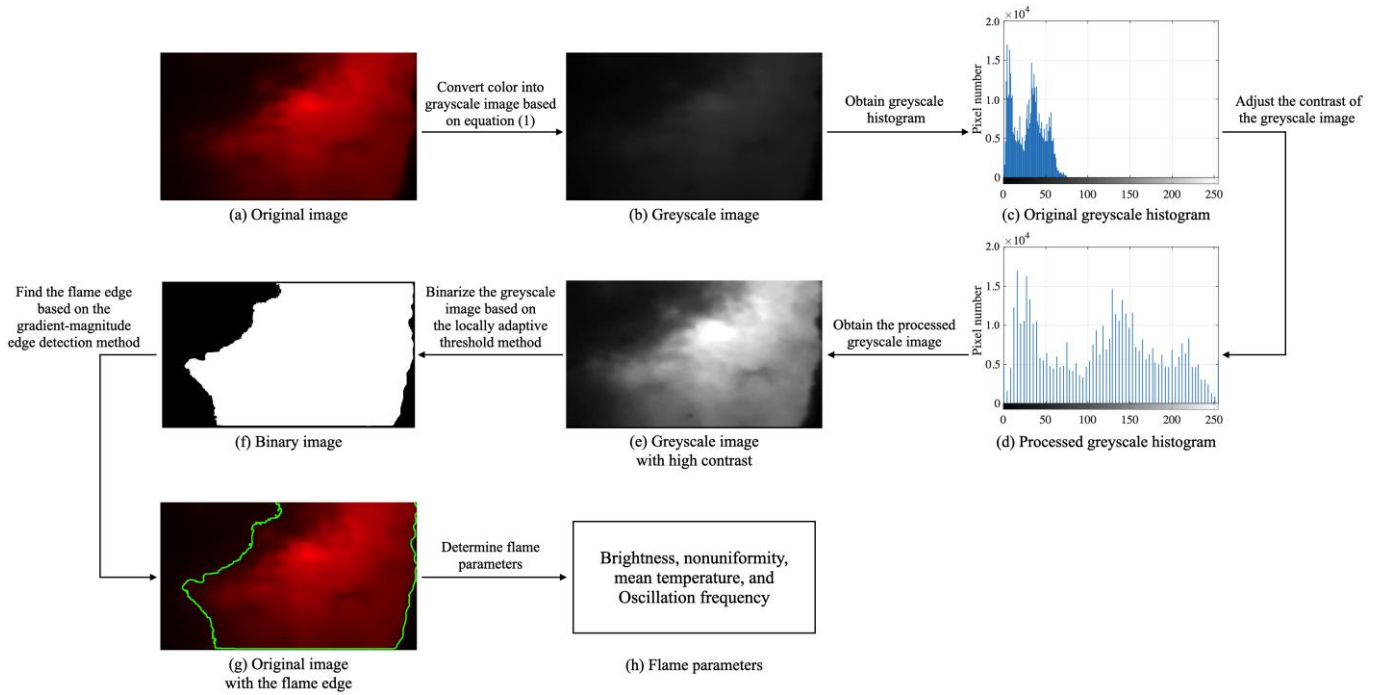
Fig. 8. Key stages in the processing of a typical flame image during the stage of constant coal feed rate.

(a) Initial reduction in coal feed rate (b) Further reduction in coal feed rate   (c) No coal feed

Fig. 9. Typical flame images with flame edges.

(a) Oscillation frequency   (b) Variability of the oscillation frequency
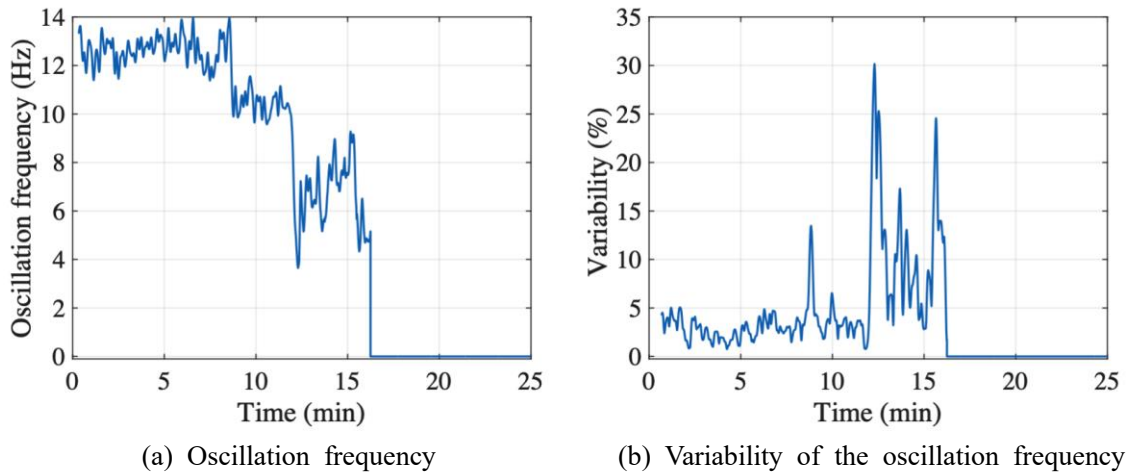
Fig. 10. Variations in the oscillation frequency and its variability with time.

Fig. 10 shows the variations in the flame oscillation frequency as well as its variability with time. Each data point in the oscillation frequency plot is obtained from 512 successive images whilst every data point in the variability graph is determined from 512 successive oscillation frequencies. The decreasing oscillation frequency and increasing variability suggest that the flame becomes unstable with time due to the progressive reduction in coal feed rate [28]. When the coal feed stops, the flame is extinguished. In this case, the flame oscillation frequency is forced to zero in the software system simply because the amplitude of the oscillation signal derived from the flame images is significantly weaker than that when the flame is present (Fig. 7). It must be noted that, internal within the image processing software, the system still returns a value of oscillation frequency due to the weak light fluctuations of the hot refractory wall in the furnace.
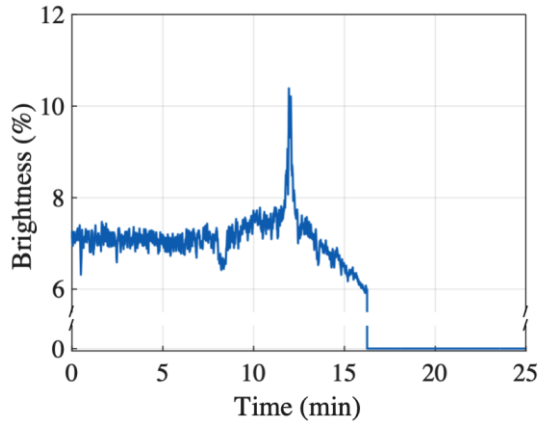
(a) Brightness
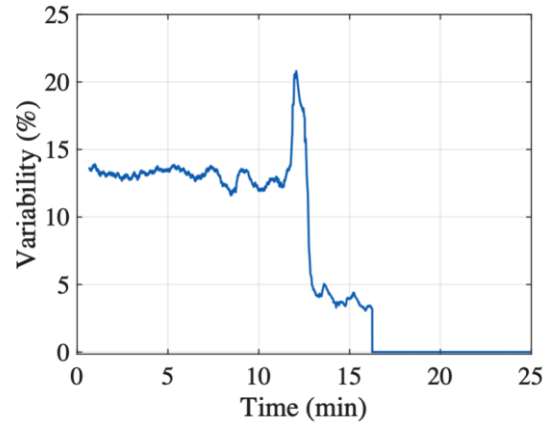
(b) Variability of the brightness

Fig. 11. Variations in the brightness and its variability with time.
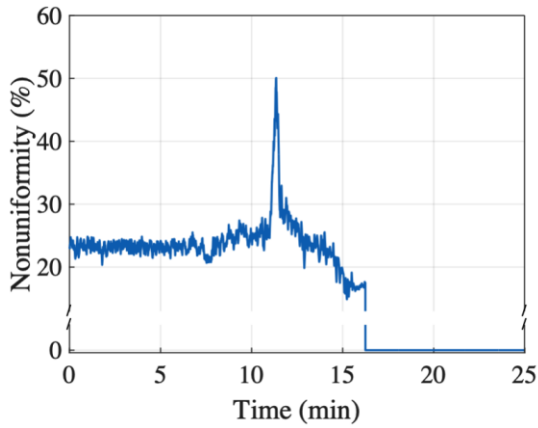
(a) Nonuniformity
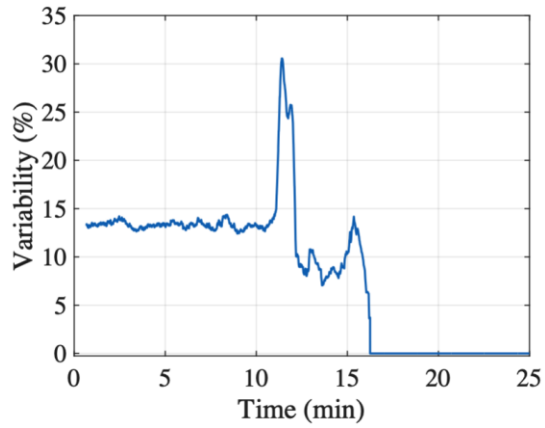
(b) Variability of the nonuniformity

Fig. 12. Variations in the nonuniformity and its variability with time.
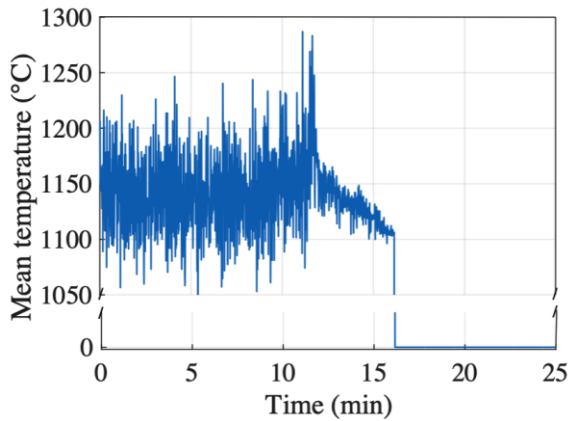
(a) Mean temperature
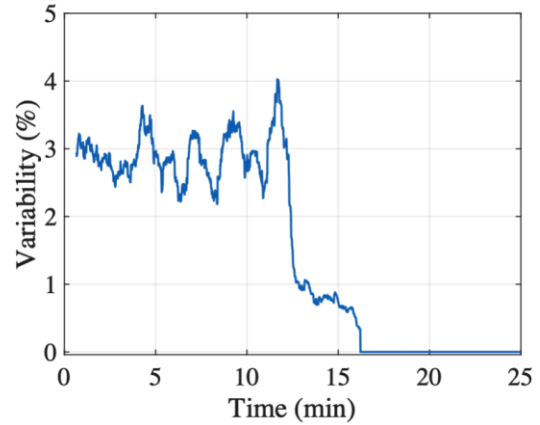
(b) Variability of the mean temperature

Fig. 13. Variations in the mean temperature and its variability with time.

Figs. 11(a), 12(a), and 13(a) depict the variations in the brightness, nonuniformity, and mean temperature with time, respectively. It is clear from Figs. 11(a) that the brightness of the flame reduces rapidly in the third stage and down to zero in the final stage because of the weak image intensity, as evidenced in Fig. 7(d) and Fig. 9(c).

It should be noted that the instantaneous value of a flame parameter is naturally fluctuating due to the inherent dynamic nature of the combustion process [37]. To obtain relatively steady flame parameters, a moving-average mechanism is applied to process the raw sequences of the four parameters, as plotted in Figs. 11(a), 12(a), and 13(a). The variations in the variability of the brightness, nonuniformity, and mean temperature with time are exhibited in Figs. 11(b), 12(b), and 13(b), respectively. Each data point in the variability plots is obtained from the raw parameter sequences with a moving window of 1024 data length.

Fig. 11 shows that with constant coal feed rate (first stage, 0 min - 11 min 30 sec), the brightness and its

(a) Before the peak time　　　　　(b) During the peak time　　　　　(c) After the peak time
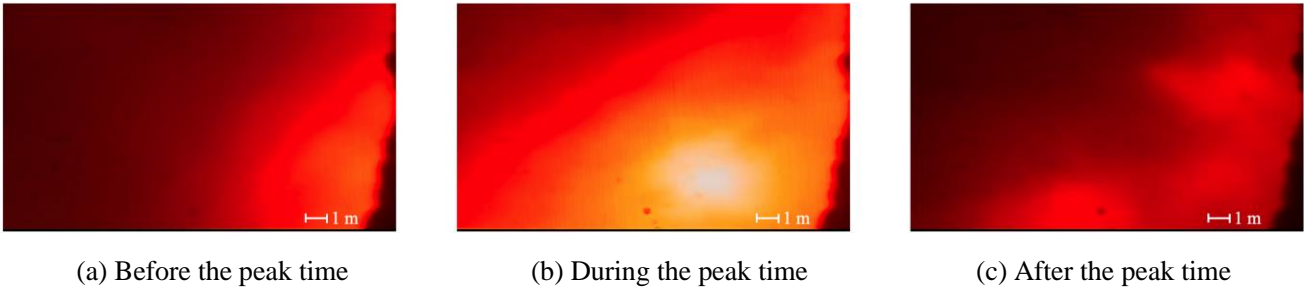
Fig. 14. Typical flame images before, during and after the peak time of the parameter variation in Figs. 11, 12 and 13.

(a) Before the peak time　　　　　(b) During the peak time　　　　　(c) After the peak time
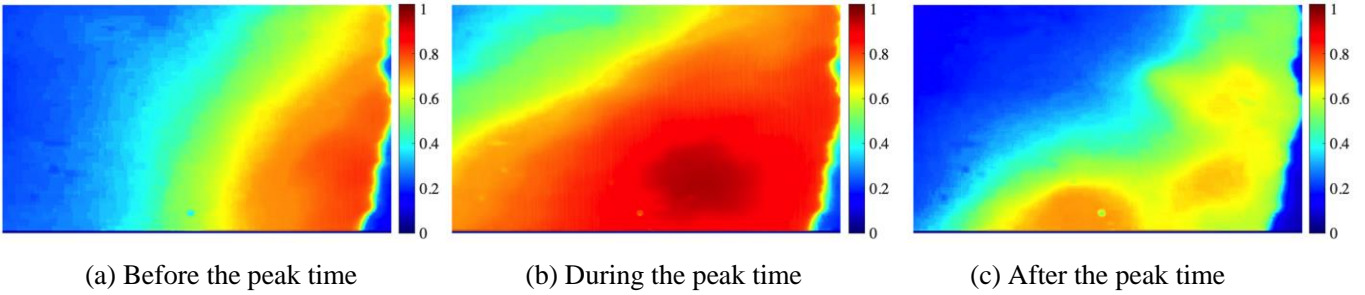
Fig. 15. Temperature distributions of the flames in Fig. 14.

variability fluctuate slightly around their means, which indicates that the flame is stable. Similar results are also obtained from the nonuniformity (Fig. 12). Additionally, although the fluctuation in the mean temperature is relatively significant (Fig. 13(a)), the average of the mean temperature remains relatively steady (Fig. 13(a)), indicating a stable flame. Such a stable flame is also represented by the magnitude of the oscillation frequency and small variability in Fig. 10.

With initial reduction in coal feed rate (second stage, 11 min 30 sec - 12 min 30 sec), the brightness, nonuniformity, mean temperature and their variability present obvious peaks, as shown in Figs. 11, 12, and 13, respectively. Typical flame images before, during and after the peak time of the parameter variations are shown in Fig. 14. The corresponding flame temperature distributions are given in Fig. 15 in the form of pseudo-colour maps. The temperature distributions are normalised to a theoretical maximum. The reason for these peaks is that the mixture of the coal and air achieves the optimal equivalence ratio for combustion with the coal feed reduced gradually [38]. The initially decreasing coal feed rate and constant air flow rate in the second stage (Fig. 5) also indicate this reason for such peaks. The complete combustion of the pulverized coal increases the flame temperature (Fig. 14) and causes the intense light emitted from the flame (Fig. 15) [38], which increases the brightness and nonuniformity as well as their variability significantly. During this stage, the oscillation frequency and its variability have a minimum

and a peak, respectively, both indicating that flame stability deteriorates rapidly.

Figs. 11(a), 12(a), and 13(a) depict that, with further reduction in coal feed rate (third stage, 12 min 30 sec - 16 min), the brightness, nonuniformity, and mean temperature decrease with time due to the insufficient fuel supply. This can be observed in Fig. 5 and Fig. 7(c) as well. The bright flame gradually dims and blurs with time. Figs. 11(b), 12(b), and 13(b) depict that the variability of the three parameters has the same decreasing trend, which indicates that the flame becomes stable. However, as shown in Fig. 10, the oscillation frequency and its variability maintain the levels achieved in the second stage, i.e. the small oscillation frequency and large variability. This suggests that the flame is unstable, which is opposite to the results from the other three parameters. This is because the
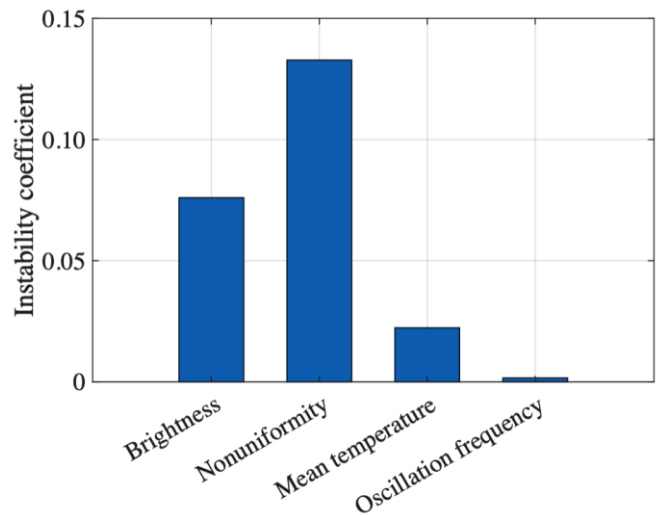
Fig. 16. Instability coefficients for the flame parameters.

decreasing coal feed rate increases the low frequency components of the flame signal due to the aerodynamics in the furnace. The oscillation frequency in this stage is mainly determined by the air flow rate, which is also supported by the excessive air flow rate, as shown in Fig. 5. Considering that the flame is nearly extinguished due to the excessive air, the oscillation frequency and its variability reflect the flame stability better than the other parameters.

Figs. 11, 12, and 13 confirm that, with no coal feed (last stage, 16 min - 25min), the brightness, nonuniformity, and mean temperature are all forced to zero as the flame is now absent. Again, within the image processing software, the system still returns values of nonuniformity and mean temperature, which are derived the images of the hot refractory wall.

Fig. 16 shows the instability coefficients of the four parameters to characterise their sensitivity to the flame stability variation, as described in Section 2.3. These coefficients are determined from the variability of the unusual values of the corresponding parameters in the first stage because the flame in this stage is the most stable. Figs. 11(b), 12(b), and 13(b) exhibit that the variability of the nonuniformity has the most significant change among the four parameters during the first three stages. Furthermore, the nonuniformity has the highest instability coefficient (Fig.16). Thus, the nonuniformity reflects the change in the flame stability better than the other three parameters in this study. This can be also observed in Fig. 7 that the difference of the luminous intensities between the 'light' and 'dark' regions changes significantly with the reduction in coal feed rate. The instability coefficient for the oscillation frequency is very low compared to the other three parameters. This is because the oscillation frequency, which is determined from multiple images (512 in this study), contains multi-aspect flame stability information and reflects flame stability over a period of time. When the flame is stable, the oscillation frequency does not have a significant change and thus its instability coefficient is very low. The other three parameters fluctuate occasionally over a wider range of values due to the inherent dynamic nature of the combustion process, leading to relatively large instability coefficients.

Figs. 17(a) and (b) exhibits the flame stability index and its standard deviation, respectively, during the shut off process. As the coal feed rate remains constant (first stage,
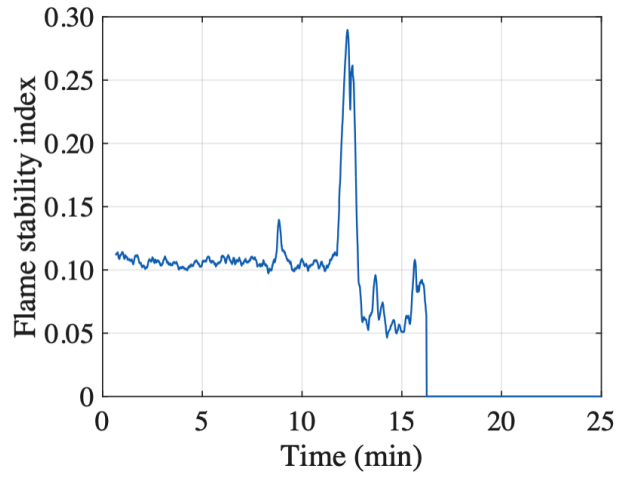
(a) Flame stability index
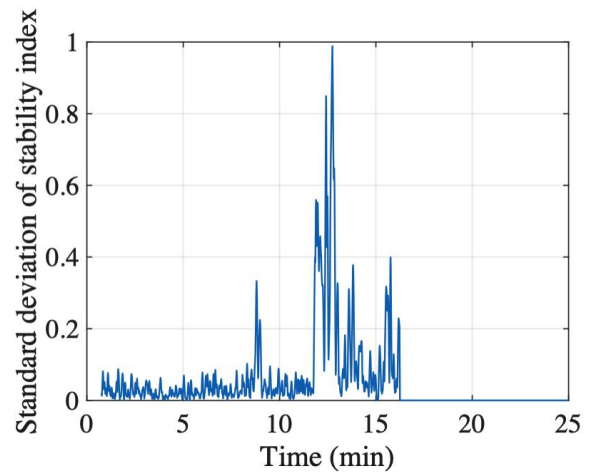
(b) Standard deviation of flame stability index
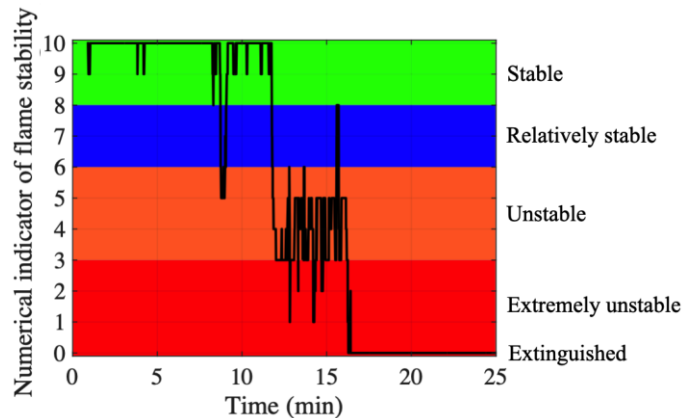
(c) Numerical indicator of flame stability

Fig. 17. Flame stability results in terms of flame stability index and numerical indicator.

0 min - 11 min 30 sec), there is no significant change in the flame stability index, indicating a stable flame, except for the 8th minute. The flame stability index at the 8th minute demonstrates the flame stability deteriorate temporarily likely due to large coal particles at that moment. With the initial reduction in coal feed rate (second stage, 11 min 30 sec - 12 min 30 sec), the flame stability index has a significant peak, indicating that the flame is unstable. With further reduction in coal feed rate (third stage, 12 min 30

sec - 16 min), the decreasing flame stability index with the large standard deviations (Fig. 17(b)), where each data point is obtained from 128 stability index, suggest that the flame fluctuates progressively towards extinction. With no apparent coal feed (last stage, 16 min - 25min), the flame stability index is 0, which is due to the fact that the flame has been extinguished in this stage.

As can be seen, although the flame stability index characterises the flame stability sensibly, its result is not straightforward enough to comprehend for the plant operators. Fig. 17(c) shows the variation in the numerical indicator of flame stability throughout the shut-down process. The four distinct colours, i.e. green, blue, orange, and red, represent four different flame states, i.e. stable, relatively stable, unstable, and extremely unstable, respectively. As the flame is extinguished in the last stage, the numerical indicator is 0. The mean and standard deviation of the flame stability index during 0 min to 7 min are 0.1064 and 0.0030, respectively. Due to the small standard deviation (Fig. 17(b)), the mean represents the best flame stability under the current combustion conditions. Based on such a mean and standard deviation, the numerical indicator of flame stability is obtained from the flame stability index. It can be seen from Fig. 17(c) that the numerical flame stability indicator presents well the flame state from stable to unstable and eventually extinguished. The colour coded flame states are the direct outputs of the flame monitoring system.

4. Conclusion

The stability of a pulverized coal flame has been measured continuously and quantitatively based on the digital imaging and image processing techniques. Results obtained on a 600 MWth coal-fired supercritical unit have demonstrated that, in a routine boiler "turning off" process, the flame stability is well characterized using the numerical indicator, which is converted and rounded from the flame stability index. The numerical indicator for flame stability changes from 10 to 1, suggesting that the flame stability deteriorates gradually with the decreasing coal feed rate. Moreover, the results have indicated that the nonuniformity is most sensitive to the change in flame stability. It has also been found that the oscillation frequency and its variability reflect better the stability of the nearly-extinguished flame than the other parameters.

References

[1] A. A. Bhuiyan, A. S. Blicblau, AKMS Islam, J. Nasera, A review on thermo-chemical characteristics of coal/biomass co-firing in industrial furnace, J. Energy Inst. 91 (2018) 1-18. https://doi.org/10.1016/j.joei.2016.10.006.

[2] R. Zhang, F. Hao, W. Fan, Combustion and stability characteristics of ultra-compact combustor using cavity for gas turbines, Appl. Energy 225 (2018) 940-954. https://doi.org/10.1016/j.apenergy.2018.05.084.

[3] J. Ballester, T. García-Armingol, Diagnostic techniques for the monitoring and control of practical flames, Prog. Energy Combust. Sci. 36 (2010) 375-411. https://doi.org/10.1016/j.pecs.2009.11.005.

[4] F. Li, H. Yang, J. Zhang, C. Gu, J. Huo, L. Jiang, X. Wang, D. Zhao, OH-PLIF investigation of Y2O3-ZrO2 coating improving flame stability in a narrow channel, Chem. Eng. J. 405 (2021) 126708. https://doi.org/10.1016/j.cej.2020.126708.

[5] W. Zhu, X. Li, J. Peng, Z. Wang, R. Sun, L. Zhang, X. Yu, Y. Yu, Study on the combustion behaviours of two high-volatile coal particle streams with high-speed OH-PLIF, Fuel 265 (2020) 116956. https://doi.org/10.1016/j.fuel.2019.116956.

[6] V. Harihara, D.P. Mishra, Dynamic flame stability diagnosis of inverse jet flame using CH* chemiluminescence, Fuel 285 (2021): 119277. https://doi.org/10.1016/j.fuel.2020.119277.

[7] Y. Zhou, F. Xie, M. Yao, X. Song, Y. Bai, G. Yu, Investigation on stability and chemiluminescence characterization for liftoff inverse diffusion flames, Combust Sci Technol 194 (2022): 2461-2479. https://doi.org/10.1080/00102202.2021.1872552.

[8] Y. Yan, Y. Hu, L. Wang, X. Qian, W. Zhang, K. Reda, J. Wu, G. Zheng, Electrostatic sensors – Their principles and applications, Measurement 169 (2021) 108506. https://doi.org/10.1016/j.measurement.2020.108506.

[9] J. Wu, Y. Yan, Y. Hu, X. Qian, G. Zheng, Oscillation frequency measurement of gaseous diffusion flames using electrostatic sensing techniques, Fuel 311 (2022) 122605.

https://doi.org/10.1016/j.fuel.2021.122605.

[10] A. Lay-Ekuakille, M. G. De Giorgia, A. Ficarella, S. Campilongo, S. Urooj, V. Bhateja, P. Sommella, C. Liguori, Advanced imaging processing for extracting dynamic features of gas turbine combustion chamber, Measurement 116 (2018) 669-675.

https://doi.org/10.1016/j.measurement.2017.11.015.

[11] S. Lu, X. Wang, H. Yu, H. Dong, Z. Yang, Trend extraction and identification method of cement burning zone flame temperature based on EMD and least square, Measurement 111 (2017) 208-215.

https://doi.org/10.1016/j.measurement.2017.07.047.

[12] W. Wojcik, A. Kotyra, P. Komada, T. Golec, Detection of combustion instabilities using the wavelet transform in industrial conditions, in Proceedings of SPIE 22 (2002) 72-76.

https://doi.org/10.1117/12.475972.

[13] J. Smart, G. Lu, Y. Yan, G. Riley, Characterisation of an oxy-coal flame through digital imaging, Combust Flame 157 (2010) 1132-1139.

https://doi.org/10.1016/j.combustflame.2009.10.017.

[14] B.B. Samantaray, C.K. Mohanta, Analysis of industrial flame characteristics and constancy study using image processing technique, J. Mech. Eng. Sci. 9 (2015) 1604-1613.

http://dx.doi.org/10.15282/jmes.9.2015.8.0156.

[15] J. Matthes, P. Waibel, M. Vogelbacher, H.J. Gehrmann, H.B. Keller, A new camera-based method for measuring the flame stability of non-oscillating and oscillating combustions, Exp. Therm. Fluid Sci. 105 (2019) 27-34.

https://doi.org/10.1016/j.expthermflusci.2019.03.008.

[16] V. H. Gaidhane, Y. V. Hote, An efficient edge extraction approach for flame image analysis, Pattern Anal Appl 21 (2018) 1139-1150.

https://doi.org/10.1007/s10044-018-0717-0.

[17] Y. Wang, Y. Yu, X. Zhu, Z. Zhang, Pattern recognition for measuring the flame stability of gas-fired combustion based on the image processing technology, Fuel 270 (2020) 117486.

https://doi.org/10.1016/j.fuel.2020.117486.

[18] J. Pan, J.A. Libera, N.H. Paulson, M. Stan, Flame Stability Analysis of Flame Spray Pyrolysis by Artificial Intelligence, Int J Adv Manuf Technol 114 (2021) 2215–2228.

https://doi.org/10.1007/s00170-021-06884-z.

[19] A. González-Cencerrado, B. Peña, A. Gil, Coal flame characterization by means of digital image processing in a semi-industrial scale PF swirl burner, Appl. Energy 94 (2012) 375-384.

https://doi.org/10.1016/j.apenergy.2012.01.059.

[20] D. Sun, G. Lu, H. Zhou, X. Li, Y. Yan, A simple index based quantitative assessment of flame stability, IEEE International Conference on Imaging Systems and Techniques (2013) 190-193.

https://doi.org/10.1109/IST.2013.6729689.

[21] M. Najarnikoo, M. Z. T, H. Pasdarshahri, Experimental study on the flame stability and color characterization of cylindrical premixed perforated burner of condensing boiler by image processing method, Energy 189 (2019) 116130.

https://doi.org/10.1016/j.energy.2019.116130.

[22] G. Lu, Y. Yan, S. Cornwell, M. Whitehouse, G. Riley, Impact of co-firing coal and biomass on flame characteristics and stability, Fuel, 87 (2008) 1133-1140.

https://doi.org/10.1016/j.fuel.2007.07.005.

[23] T. Chi, H. Zhang, Y. Yan, H. Zhou, H. Zheng, Investigations into the ignition behaviors of pulverized coals and coal blends in a drop tube furnace using flame monitoring techniques, Fuel 89 (2010) 743-751.

https://doi.org/10.1016/j.fuel.2009.06.010.

[24] M. G. De Giorgi, A. Sciolti, S. Campilongo, A. Ficarella, Image processing for the characterization of flame stability in a non-premixed liquid fuel burner near lean blowout, Aerosp Sci Technol 49 (2016) 41-51.

https://doi.org/10.1016/j.ast.2015.11.030.

[25] T. Qiu, M. Liu, G. Zhou, L. Wang, K. Gao, An unsupervised classification method for flame image of pulverized coal combustion based on convolutional auto-encoder and hidden Markov model, Energies 12 (2019) 2585.

https://doi.org/10.3390/en12132585.

[26] D. Sun, G. Lu, Y. Yan, An embedded imaging and signal processing system for flame stability monitoring and characterization, 2010 IEEE International

Conference on Imaging Systems and Techniques, (2010) 210-213.

https://doi.org/10.1109/IST.2010.5548471.

[27] D. Sun, G. Lu, H. Zhou, X. Li, Y. Yan, A simple index based quantitative assessment of flame stability, 2013 IEEE International Conference on Imaging Systems and Techniques, (2013) 190-193.

https://doi.org/10.1109/IST.2013.6729689.

[28] W. Xu, Y. Yan, G. Lu, X. Bai, Quantitative assessment of burner flame stability through digital image processing, IEEE Trans Instrum Meas 71(2022) 5021913.

https://doi.org/10.1109/TIM.2022.3205671.

[29] J. Yang, Z. Ma, Y. Zhang, Improved colour-modelled CH* and C2 * measurement using a digital colour camera, Measurement 141 (2019) 235-240.

https://doi.org/10.1016/j.measurement.2019.04.016.

[30] S. G. Sahu, N. Chakraborty, P. Sarkar, Coal–biomass co-combustion: An overview, Renew. Sust. Energ. Rev. 39 (2014) 575-586.

https://doi.org/10.1016/j.rser.2014.07.106.

[31] A. Zacco, L. Borgese, A. Gianoncelli, R. P. W. J. Struis, L. E. Depero, E. Bontempi, Review of fly ash inertisation treatments and recycling, Environ Chem Lett 12 (2014) 153-175.

https://doi.org/10.1007/s10311-014-0454-6.

[32] P. R .N. Childs, J. R. Greenwood, C. A. Long, Review of temperature measurement, Rev. Sci. Instrum. 71 (2000) 2959-2978.

https://doi.org/10.1063/1.1305516

[33] G. Lu, Y. Yan, M. Colechin, R. Hill, Monitoring of oscillatory characteristics of pulverized coal flames through image processing and spectral analysis, IEEE Trans Instrum Meas, 55 (2006) 226-231.

https://doi.org/10.1109/TIM.2005.861254

[34] C. Saravanan, Color image to grayscale image conversion, 2010 Second International Conference on Computer Engineering and Applications, (2010) 196-199.

https://doi.org/10.1109/ICCEA.2010.192.

[35] D. Bradley, G. Roth, Adapting thresholding using the integral image, Journal of Graphics Tools 12 (2007) 13–21.

https://doi.org/10.1080/2151237X.2007.10129236.

[36] O. R. Vincent, O. Folorunso, A descriptive algorithm for sobel image edge detection, Proceedings of informing science & IT education conference 40 (2009) 97-107.

https://doi.org/10.28945/3351.

[37] G. Lu, Y. Yan, M. Colechin, A digital imaging based multifunctional flame monitoring system, IEEE Trans Instrum Meas 53 (2004) 1152-1158.

https://doi.org/10.1109/TIM.2004.830571.

[38] L. Chen, S. Yong, A.F. Ghoniem, Oxy-fuel combustion of pulverized coal: Characterization, fundamentals, stabilization and CFD modeling, Prog. Energy Combust. Sci. 38 (2012) 156-214.

https://doi.org/10.1016/j.pecs.2011.09.003.